Recent advances in germanium emission

P. Boucaud,[1,*] M. El Kurdi,[1] A. Ghrib,[1] M. Prost,[1,2] M. de Kersauson,[1] S. Sauvage,[1] F. Aniel,[1] X. Checoury,[1] G. Beaudoin,[3] L. Largeau,[3] I. Sagnes,[3] G. Ndong,[4] M. Chaigneau,[4] and R. Ossikovski[4]

[1]*Institut d'Electronique Fondamentale, CNRS—Univ. Paris Sud 11, Bâtiment 220, F-91405 Orsay, France*
[2]*STMicroelectronics, 850 rue Jean Monnet, 38920 Crolles, France*
[3]*Laboratoire de Photonique et de Nanostructures, CNRS—UPR 20, Route de Nozay 91460 Marcoussis, France*
[4]*Laboratoire de Physique des Interfaces et des Couches Minces, CNRS—Ecole polytechnique, F-91128 Palaiseau, France*
**Corresponding author: philippe.boucaud@ief.u-psud.fr*

Received March 29, 2013; revised June 12, 2013; accepted June 21, 2013;
posted July 5, 2013 (Doc. ID 187998); published August 13, 2013

The optical properties of germanium can be tailored by combining strain engineering and *n*-type doping. In this paper, we review the recent progress that has been reported in the study of germanium light emitters for silicon photonics. We discuss the different approaches that were implemented for strain engineering and the issues associated with *n*-type doping. We show that compact germanium emitters can be obtained by processing germanium into tensile-strained microdisks.

OCIS codes: (160.6000) Semiconductor materials; (230.0250) Optoelectronics; (300.6280) Spectroscopy, fluorescence and luminescence.
http://dx.doi.org/10.1364/PRJ.1.000102

1. INTRODUCTION

Germanium is a semiconductor with an indirect bandgap. The energy difference between the minimum of the conduction band corresponding to the L valley in the reciprocal space and the zone center Γ valley is only 140 meV at room temperature, a value significantly smaller than the one for silicon (electron volt range). This reasonably small difference allows one to observe direct bandgap recombination under optical or electrical injection at room temperature, since the zone center Γ valley is thermally populated. In germanium with weak n-doping, the fraction of the carrier population in the Γ valley is 4 orders of magnitude smaller than the population of the L valley. But the direct bandgap recombination is far more efficient than the indirect bandgap recombination, which requires additional particles such as phonons or scattering mechanisms to respect the wave-vector conservation rule. It was reported as early as 1955 that the room temperature amplitude of direct bandgap recombination of germanium can be larger than the indirect bandgap recombination [1,2]. At low temperature, the thermal population of the Γ valley vanishes, and the optical recombination is dominated by phonon-assisted recombination [3]. Population of the zone center Γ valley remains possible even at low temperature, as Auger scattering mechanisms can assist transfer of carrier population from the L valley to the Γ valley under strong optical pumping [4].

A very important characteristic of germanium is that the direct bandgap energy is close to 1.55 μm at room temperature. This property was exploited largely in order to develop light photodetectors directly fabricated on silicon. Germanium was indeed first introduced in a silicon process through silicon–germanium alloys, in particular for the development of heterostructure bipolar transistors. Germanium, as a group IV element, is fully compatible with the complementary metal oxide semiconductor (C-MOS) environment. This explains the strong interest for germanium-based detection in the transparency window of silicon around 1.55 and 1.3 μm [5–7]. These photodetectors can operate at very high frequency and are now building blocks in the silicon photonics environment.

The interest of germanium as a potential integrated emitter for silicon photonics was only recognized recently. Resonant emission around the 1.55 μm telecom wavelength is certainly a strong asset. However, even if the energy difference between the L and Γ valley is only around 140 meV, the weak carrier population in the Γ valley appears as a significant hurdle for obtaining efficient emission. Emitters based on indirect bandgap recombination can exhibit reasonably high quantum efficiency, providing that nonradiative recombination mechanisms are quenched and that the external coupling or extraction of photon emission is optimized [8]. Even if stimulated emission can be in principle achieved with indirect bandgap materials [9], one needs to consider the balance between gain and free-carrier absorption, the latter turning out to be the dominant term under very high optical pumping. A germanium-based integrated and efficient emitter should thus rely on the direct bandgap recombination. The energy difference between conduction valleys depends on the strain applied to the material as the deformation potential coefficients vary between the different bands. It was shown that tensile strain can reduce the energy splitting between the L and the Γ valley [10], and germanium can even become a direct bandgap material for a tensile strain around 2%. It is clear that the smaller the splitting between L and Γ valleys, the larger the external quantum efficiency that could be achieved, the external quantum efficiency being defined as the ratio between the number of collected photons and the number of injected electron–hole pairs. Another ingredient to enhance the optical recombination is to introduce n-type doping in germanium. The n-type doping raises the Fermi level into the conduction band. The carrier density needed to reach optical

transparency is, as a consequence, decreased. It means that fewer electrons and consequently fewer holes need to be injected to obtain a positive optical gain. The reduction in the hole density is important, as the hole free-carrier absorption cross section is larger than the electron free-carrier absorption cross section and might possibly cancel the optical gain.

By combining tensile strain and n-type doping, one expects optical gain to be obtained in germanium. Experimentally, a germanium-based laser was first demonstrated under optical pumping at room temperature [11]. More recently, lasing under electrical injection has been reported by the same group [12]. These two results highlight the potential that germanium represents as a monolithic integrated optical source on silicon. It explains the interest of many groups to investigate the optical properties of germanium and the development of many approaches to enhance the optical recombination properties. In this paper, we will review the recent progress reported in that field. We discuss the modeling of optical gain and the issue of n-type doping and free-carrier absorption. We report experimental infrared absorption measurements on doped germanium and find no evidence of L to Γ absorption increasing from 10 to 2 μm. We discuss the several approaches that have been used to apply tensile strain on germanium. We show the interest of germanium microdisks as compact emitters. We finally discuss electrical injection in Ge/GaAs heterostructures.

2. MODELING OF GERMANIUM OPTICAL GAIN

Several groups have theoretically investigated the properties of n-doped tensile-strained germanium. Liu *et al.* first showed, using an effective mass formalism, that a 0.25% tensile-strained germanium with 7.6×10^{19} cm^{-3} n-type doping could exhibit a 400 cm^{-1} net gain, the net gain being the difference between optical gain and free-carrier absorption, at room temperature [13]. The theory of optical gain in Ge-SiGeSn quantum well lasers was developed by Chang and Chuang [14]. The effective mass approach presents limitations for an accurate description of the density of states. It explains why other approaches were implemented in order to calculate the optical gain, either by a tight-binding formalism [15] or a multiband $\mathbf{k}\cdot\mathbf{p}$ formalism [16]. An $sp^3d^5s^*$ tight-binding model was implemented in [17] in order to calculate the band structure of strained germanium and investigate the trade-off between n-type doping and tensile strain for the highest efficiency. The effect of crystal orientation was investigated in [18]. The models indicate that even a 0.25% tensile strain is sufficient to obtain positive gain in strongly doped germanium, whereas it is not possible in unstrained intrinsic germanium [19]. The interest of tensile strain to lower the requirement on carrier density to achieve optical transparency is thus obvious. Figure 1 shows the calculated dependence of the carrier density needed to reach optical transparency, i.e., compensation of internal losses by internal gain, as a function of tensile strain. The calculation is performed with our 30 band $\mathbf{k}\cdot\mathbf{p}$ formalism [16]. The n-type doping of germanium considered here is 2×10^{19} cm^{-3}. One can see that the effect of tensile strain is significant, as it leads to a regular decrease of the carrier density that needs to be optically or electrically injected. For a 0.7% biaxial strain, the carrier density is only 3.5×10^{18} cm^{-3} to reach optical transparency at room temperature if we consider the free-carrier absorption as reported in [13]. Beyond the accurate description of tensile-strained germanium band structure, the free-carrier absorption that is taken into account is a very important parameter, as it can significantly modify the amplitude of the optical gain. The effect of free-carrier absorption is discussed in the next section. The requirement on photoinduced carrier density to obtain transparency can be significantly more challenging if the free-carrier absorption is stronger, as seen in Fig. 1. We note that the tensile strain shifts the recombination resonance to a longer wavelength. This is a direct consequence of the energy decrease of the Γ valley and the splitting between the heavy hole and light hole bands. While this effect might be considered as strongly negative, it can nonetheless be circumvented by applying tensile strain as well to the detection devices, like germanium-on-silicon photodetector, in a future germanium photonics platform.

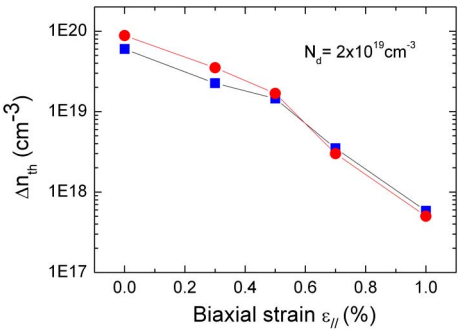

Fig. 1. Calculated dependence of photoinduced carrier density needed to reach transparency at room temperature in n-doped germanium as a function of tensile strain. The germanium doping is 2×10^{19} cm^{-3}. The calculation is based on the 30-band $\mathbf{k}\cdot\mathbf{p}$ formalism that we presented in [16]. The squares account for free-carrier absorption, as reported in [13]. The circles correspond to a calculation that considers the experimental absorption cross section for electrons and holes reported in [20] and a power law dependence as a function of wavelength with an exponent of 2.25 for electrons and 2.43 for holes.

3. n-TYPE DOPING AND FREE-CARRIER ABSORPTION

The n-type doping of germanium allows one to reduce the carrier density that needs to be injected in order to obtain optical gain. The doping raises the Fermi energy and leads to a superlinear increase of the carrier density present in the Γ valley. It thus leads to an enhanced direct bandgap recombination. This effect was confirmed by studying the amplitude of the radiative recombination as a function of the doping level, and good agreement was found with the modeling that accounts for the carrier distribution [21,22]. This enhanced efficiency might, however, be counterbalanced by the increase of nonradiative recombination as the doping level is increased [23,24]. Doping has a major effect on the Schockley–Read–Hall recombination mechanisms, and the Schockley–Read–Hall lifetime can be decreased by several orders of magnitude as the doping is increased. At high doping level, the Schockley–Read–Hall lifetime can even reach the same range as the Auger recombination time. High doping might thus decrease the internal efficiency. The second drawback of high doping is related to free-carrier absorption. Free-carrier absorption in n-doped germanium was studied in the 1960s [25–27]. The effect of impurities on free-hole absorption was discussed by Newman

and Tyler [28]. The data of Newman and Spitzer were empirically fitted by Liu *et al.* [13] in order to obtain practical formula for gain calculation. The free-carrier absorption is linearly proportional to the electron or hole carrier density and exhibits a wavelength dependence that varies for electrons and holes. Between 1500 and 1600 nm, Liu *et al.* estimated that the free-hole absorption cross section was about 4 times larger than the free-electron-carrier absorption. Photoinduced free-carrier absorption in germanium was also investigated by Carroll and co-workers [20]. For electrons, the experimentally measured absorption cross section was smaller than the one reported in [13] (by a factor of 1.9 if extrapolated at 1650 nm). Carroll *et al.* did extrapolate the same electron absorption cross section, i.e., one consistent with their results, from the data of [25]. However, the absorption cross section was found to be significantly larger for free holes (by a factor of 1.8 as compared to the data quoted in [13] around 1650 nm) and this was attributed to the role of valence intraband absorption between heavy holes and the spin-orbit split-off band that was possibly underestimated by Liu *et al.* Carroll and co-workers have deduced that the underestimation of free-hole absorption relieves the constraints to achieve germanium lasing. Their conclusion was that for their conditions it was not possible to obtain positive optical gain, as free-carrier absorption always dominates optical gain. The free-carrier absorption associated with both n-doping and photoinduced carriers is a central parameter to predict whether lasing can be obtained. This has to be considered in view of the investigated sample geometries and the role of nonradiative and surface recombinations for photoinduced carriers, as well as the quality of the layers. Impurity content might vary between samples and lead to different nonradiative recombinations as well as different scattering mechanisms for free-carrier absorption. We note that nonradiative processes can also have a direct effect on the recombination spectral shape [29].

The measurement of germanium absorption over the infrared spectral range with very thin films with thicknesses lower than 1 μm is not a trivial issue. Wang and co-workers have analyzed the infrared absorption of tensile-strained n-type germanium grown on a single-side polished silicon wafer [30]. In a normal incidence geometry, a significant modulation of the transmitted signal is present due to Fabry–Perot oscillations with a variable periodicity over the infrared spectral range. The transmission strongly depends on the backside scattering if single-side polished wafers are used. We have performed transmission infrared measurements using samples grown on double-side polished wafers. The investigated germanium sample was grown on a GaAs wafer that is closely lattice matched to germanium. No defects are thus present at the interfaces, and only a residual compressive strain (0.07%) is present in the sample. The growth is performed in a metal-organic chemical vapor deposition chamber [31]. The doping level is around 10^{19} cm^{-3}. Figure 2(a) shows the transmission spectra measured in a Fourier transform infrared spectrometer with different beam splitters in order to cover a large spectral range. The transmission is normalized by the transmission of a double-side polished GaAs wafer identical to the one used for epitaxy. The infrared spectrum is thus the direct signature of the germanium film optical properties. Clear Fabry–Perot oscillations with a significant amplitude

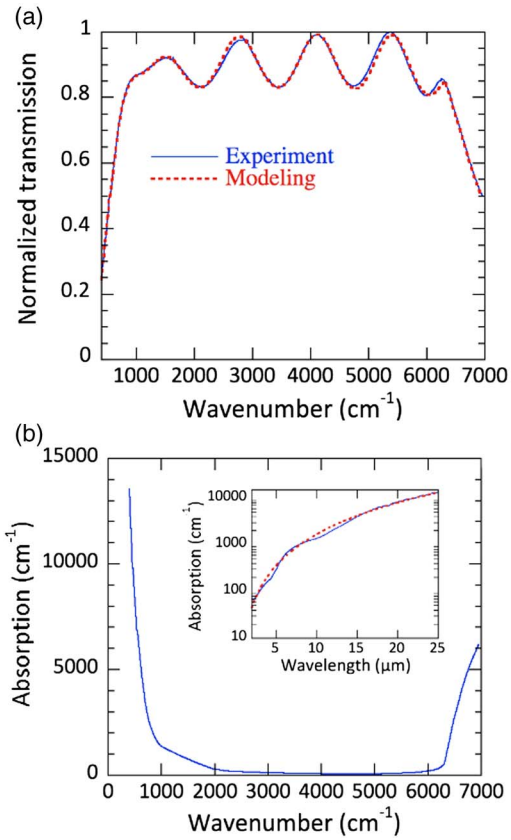

Fig. 2. (a) Transmission of a Ge/GaAs film normalized by the transmission of a GaAs wafer. Both wafers are double-side polished. The germanium thickness is 930 nm. The doping of the germanium layer is 10^{19} cm^{-3}. The germanium absorption is deduced from this normalized transmission. The dashed line corresponds to the modeling of the transmission that accounts for the germanium absorption. (b) Absorption of the germanium film as a function of wavenumber. The inset shows a zoom of the absorption in the 2–25 μm spectral range. The dashed line corresponds to a power fit with a 2.25 exponent (absorption $\propto \lambda^{2.25}$).

can be observed on the spectrum. The amplitude depends on both absorption amplitude and index contrast between germanium and GaAs. One can deduce the germanium absorption coefficient from this transmission spectrum. Figure 2(b) shows the deduced absorption amplitude that results from both free-carrier absorption as well as direct and indirect bandgap absorption. The simulated transmission using these data is superimposed on the experimental transmission of Fig. 2(a). At 500 cm^{-1} (20 μm), the absorption coefficient is 8300 cm^{-1}. The absorption increases continuously from 2 to 25 μm. From 2 to 25 μm, the absorption can be well fitted following a power law dependence with an exponent of 2.25 (see inset of Fig. 2), not very different from the λ^2 dependence that is usually quoted for free-carrier absorption following a Drude model. This power law exponent for electron absorption corresponds to the one quoted by Liu *et al.* in [13]. The prefactor for this power law dependence is around two times smaller than the one reported in [13] and in agreement with the measured value reported for electrons in [20]. The absorption spectral shape characterized by a regular increase from 2 to 25 μm is very similar to those reported, for example, in [25–27]. Our measurements show that for this sample there is no breaking down of the standard free-carrier absorption

model. As opposed to what is reported in [30], we do not observe an increase of absorption from 10 to 2 μm, the latter being attributed to L–Γ intervalley absorption. This observation could be the consequence of using single-side polished wafers with a wavelength-dependent light scattering. It is surprising for the L to Γ intervalley absorption to continuously increase up to 2 μm for a 10^{19} cm^{-3} doping level. One should rather expect a resonant transition with a maximum that is linked to the intervalley energy difference (140 meV for germanium) as shown, for example, in Fig. 7 of [32] for the specific case of GaAs.

4. APPROACHES TO APPLY TENSILE STRAIN

As illustrated in Fig. 1 and discussed in the references cited in Section 2, tensile strain applied to germanium is expected to enhance the optical gain and decrease the threshold for lasing. Growing germanium directly on silicon results in a tensile strain in germanium, because of the difference between the thermal dilatation coefficient of both materials, but with a limited amplitude of 0.2%–0.25% [33]. In order to apply larger tensile strains, different approaches have been investigated. One of the first approaches proposed was the heteroepitaxial growth of germanium on relaxed GeSn buffer layers [34,35]. In Ref. [35], germanium is the active medium. This approach is different from the one that relies on the use of germanium–tin alloys as the active gain medium [36–38]. Although the incorporation of tin is not straightforward, very significant progress has been achieved in this field, and this approach is very attractive. Moreover, it offers the possibility to engineer quantum well heterostructures, which could significantly decrease laser threshold. An alternative approach is the use of III–V metamorphic buffer layers with a lattice constant larger than that of germanium [31,39,40]. An example is the growth on lattice-mismatched $In_{1-x}Ga_xAs$ alloys, which allows one to tailor the strain by varying the indium content in the alloy. Very high strain, up to 2.33%, can be achieved with thin layers of a few nanometers [41,42]. In the latter case, the low-temperature photoluminescence properties were correlated to the occurrence of a direct bandgap for the strained material. There is, however, a trade-off between the maximum strain that can be achieved and the thickness of the strained layer. One has to avoid plastic relaxations while increasing the thickness in order to obtain a large overlap between a guided mode and the strained film. We have shown that biaxial tensile strain up to 0.75% can be obtained in germanium films for thicknesses up to 150 nm [43]. At larger thicknesses and/or larger applied strain, a deviation from tetragonal deformation is observed. One of the challenges of this approach is linked to the transfer of defects from the buffer layer to the germanium film at high tensile strain. Defects can decrease the radiative efficiency and, depending on their time dynamics, can lead to some blinking of the emission.

The use of micromechanical strain engineering and the use of an external stressor to strain bulk material or nanomembranes have also been demonstrated [42,44–47]. The use of silicon nitride as a stressor layer is certainly a very attractive possibility because of its compatibility with a C-MOS processing environment and the flexibility that it offers to control the stress transfer and to achieve high tensile strain [49–52]. An initially compressively strained silicon nitride layer deposited by plasma-enhanced chemical vapor deposition can relax and efficiently transfer its stress to germanium, as it is free to move laterally. The stress transfer will depend on the device geometry. In [51], a uniaxial strain of 1% was demonstrated in germanium photonic wires. The value can be increased up to 1.6% if the ridge waveguide is underetched. The orientation of the waveguide along [100] or [110] directions is important, as it has an effect on the band structure and the carrier population in the Γ valley. In order to demonstrate high biaxial strain using silicon nitride stressors, we have investigated the optical properties of germanium microdisks [53]. The microdisks were first fabricated from a germanium film grown on GaAs. A silicon nitride film is then deposited on the processed sample. Figure 3(a) shows a scanning electron microscopy

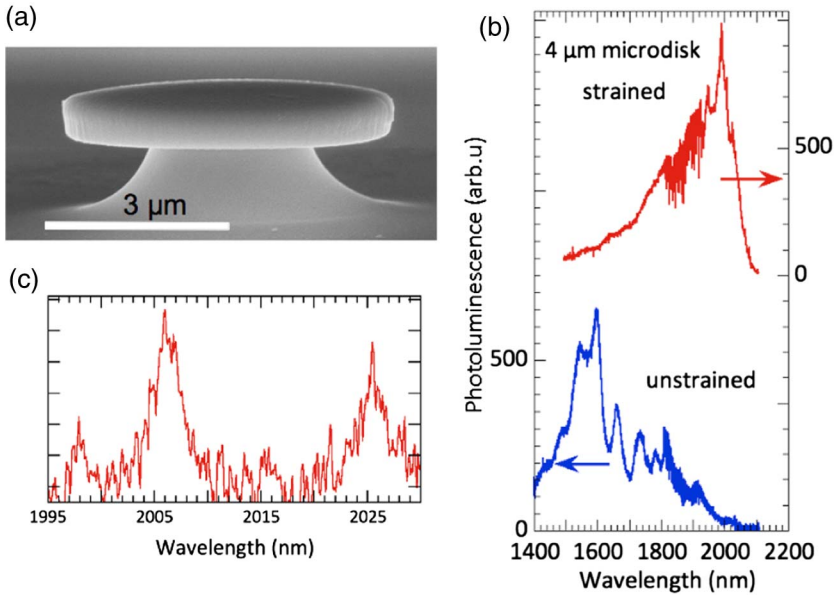

Fig. 3. (a) Scanning electron microscopy image of tensile-strained germanium microdisk. (b) Room temperature photoluminescence spectrum of an unstrained (bottom) and strained (top) germanium microdisk with a 4 μm diameter. (c) Enlargement of the emission around 2000 nm [48].

image of a strained germanium microdisk that is encapsulated by a silicon nitride film. The effect of strain can be directly observed by looking at the room temperature photoluminescence of the microdisks. Figure 3(b) shows the spectra obtained for strained and unstrained microdisks with a 4 μm diameter. For the unstrained disk, the emission is maximum around 1545 nm. The low-energy part of the spectrum below the direct bandgap is modulated by Fabry–Perot modes resulting from interferences along the disk diameter [54]. The periodicity of the modes varies with the disk diameter as expected (not shown). For the strained microdisks, the emission is redshifted with a maximum around 1990 nm for the 4 μm diameter disk. This redshift is a direct consequence of the large tensile strain present in the germanium. The redshift varies for different disk diameters, since the transferred strain depends on the size of the pedestal. This effect is confirmed by finite element modeling of the strain profile in the germanium film. Based on the same finite element modeling of the strain transfer and on the modeling of the photoluminescence spectra, we estimate a biaxial tensile strain around 1% in the 4 μm microdisk.

We have further investigated the strain distribution at the top of germanium microdisks by spatially-resolved μ-Raman (micro-Raman) spectroscopy. A high-spectral-resolution Raman spectrometer (Labram HR800 from HORIBA Jobin Yvon) was operated in confocal backscattering configuration using a 532 nm wavelength excitation from an external laser. A 100× objective (NA = 0.9) was used. The sample was mounted on a motorized xy stage enabling a 500 nm step μ-Raman mapping. In normal backscattering geometry only the longitudinal optical (LO) phonon of the Ge–Ge lattice vibration is measured, in virtue of the Raman selection rules. The frequency shift of the line of this LO mode from its

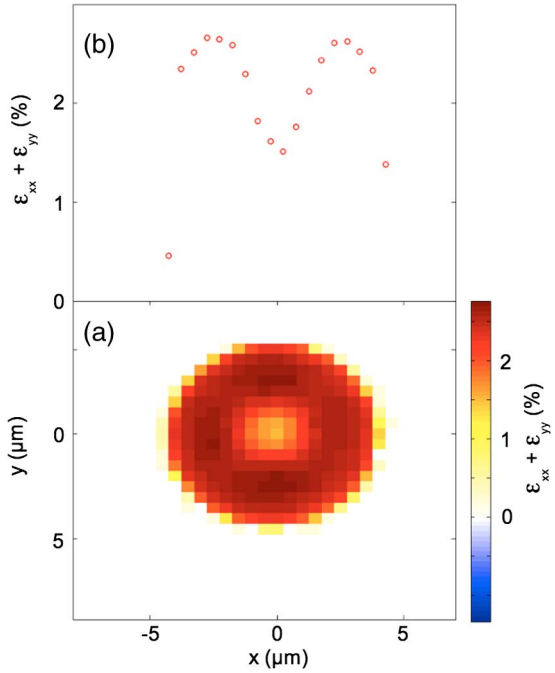

Fig. 4. (a) In-plane strain map of the germanium microdisk as deduced from backscattering μ-Raman spectroscopy. (b) Strain profile along the disk diameter. The disk diameter is 9 μm. The figure highlights the sum of the in-plane strain components. In Fig. 1, only one component is considered to describe the strain.

unstrained value (~301 cm^{-1}) is directly proportional to the sum of the in-plane strain components ε_{xx} and ε_{yy} of the germanium lattice [55,56]. Figure 4(a) shows a map of the in-plane strain distribution ($\varepsilon_{xx} + \varepsilon_{yy}$) over the microdisk surface for a 9 μm disk diameter. The magnitude of the tensile strain increases radially from the disk center outwards (from 1.51% to 2.66%) until an abrupt drop (down to below 1%) takes place at the disk edge. In this figure, we have highlighted the sum of the diagonal strain components as the Raman shift is directly proportional to this quantity. The corresponding in-plane tensile strain that is usually quoted for a merely biaxial strain has to be divided by a factor of 2, i.e., the 2.66% value corresponds to a 1.33% biaxial strain. A line scan along the disk diameter is displayed in Fig. 4(b). We note that the penetration depth of the 532 nm laser in germanium is ~20 nm, but the mode volume probed by the photoluminescence is much larger.

A nitride stressor layer is thus very efficient to transfer a high biaxial strain into germanium. Whispering gallery modes were observed on unstrained and strained microdisks. Figure 3(c) shows an enlargement of the emission around 2000 nm. Narrow modes are observed with quality factors that can reach 1000. Quality factors up to 1350 were observed in unstrained microdisks. The value of the quality factor is limited by free-carrier absorption. One of the issues associated with silicon nitride stressor is the inhomogeneity of the transferred tensile strain as a function of the vertical direction. In the case of microdisks, this inhomogeneity can be controlled by the size of the disk pedestal, a micropillar, leading to a more homogeneous strain in the germanium volume at the expense of a reduced strain amplitude. Such a configuration could ensure a better overlap between a whispering gallery mode and the tensile-strained region where optical gain is obtained. These microdisks are thus potential candidates to realize compact germanium lasers. We emphasize that the study of microdisks or suspended membranes is very sensitive to thermal dissipation. The temperature of suspended membranes can rapidly become very high (hundreds of degrees Celsius) if they are optically pumped with lasers with a few milliwatts. We have recently shown that thermal emission can become the dominant mechanism governing the recombination [57]. This thermal emission can exhibit a very strong superlinear dependence as a function of the incident power. The spectra presented above were measured with a weak power density in order to avoid this regime.

5. ELECTRICAL INJECTION

The issue of electrical injection in germanium has been addressed as early as the 1950s [1]. For silicon photonics, a monolithic optical source based on germanium can be integrated only if the source can be operated under electrical injection. Several groups have recently reported the study of germanium electroluminescent diodes [58–63]. Lasing has been reported in highly doped germanium directly deposited on silicon [12]. In the latter case, the current threshold was very high and the operation time for the lasers was very short. One of the easiest possibilities to decrease the laser threshold and to strengthen the reliability of the devices is to implement electrical injection in tensile-strained structures. First reports have already been published towards this direction [46,64]. Another important approach is the use of heterostructures

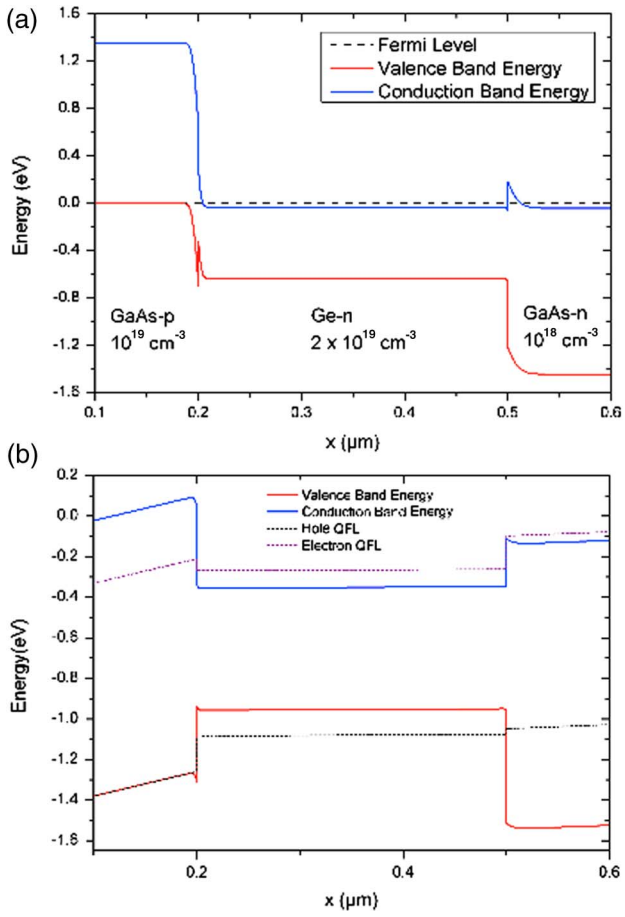

Fig. 5. (a) Conduction band profile of a GaAs/Ge/GaAs heterostructure without applied bias. (b) Conduction band profile for a 1.5 V applied bias. The quasi-Fermi levels are indicated by dashed lines.

to obtain the population inversion more easily. The growth of germanium on GaAs and the subsequent capping of germanium by doped GaAs can provide interesting structures to study germanium lasing under electrical injection. One of the advantages is the high optical quality of the heterostructure and the absence of intermediate defect layers. In this type of heterostructure, one has to consider the transfer of carriers from the Γ to the L valley, just as carriers from Δ to L must be considered for Ge/Si heterostructures. Figure 5 shows the band diagram of such heterostructure with unstrained germanium at 0 bias and under a 1.5 V bias. The doping of the 300 nm thick germanium layer is 2×10^{19} cm^{-3}. The n- and p-dopings of GaAs are 10^{18} and 10^{19} cm^{-3} respectively. The quasi-Fermi level in the germanium conduction band is 53 and 74 meV above the L minimum for an injected current density of 100 and 500 kA cm^{-2}, respectively. These values are expected to be reduced if the germanium doping is increased. Applying a tensile strain to germanium remains a prerequisite in order to decrease the threshold current of these structures.

6. CONCLUSION

Germanium has generated very strong interest because it might be used to develop a monolithic integrated optical source for silicon photonics. This integration will be successful only if the external quantum efficiency is boosted and thresholds for lasing operation are significantly reduced. Applying significant tensile strain beyond the 0.2%–0.25% obtained by direct growth on silicon is mandatory. Many different options are available for strain engineering, and it is likely that significant progress will be reported in the coming years. The electrical injection represents a major challenge. This domain is expected to be the center of intense research activity in the coming years.

ACKNOWLEDGMENTS

This work was supported by "Triangle de la Physique" under the Gerlas convention and by Agence Nationale de la Recherche under the GRAAL convention (ANR Blanc call 2011 BS03 004 01). We acknowledge the support of STMicroelectronics (F. Boeuf) through a CIFRE funding for M. Prost. G. Ndong gratefully recognizes ANRT CIFRE no. 1077/2010 Ph.D. fellowship with HORIBA Jobin Yvon. This work was also partly supported by the RENATECH network and conseil général de l'Essonne.

REFERENCES

1. J. R. Haynes, "New radiation resulting from recombination of holes and electrons in germanium," Phys. Rev. **98**, 1866–1868 (1955).
2. Y. P. Varshni, "Band-to-band radiative recombination in groups IV, VI and III–V semiconductors (I)," Phys. Status Solidi B **19**, 459–514 (1967).
3. G. A. Thomas, E. I. Blount, and M. Capizzi, "Indirect recombination mechanisms in germanium," Phys. Rev. B **19**, 702–718 (1979).
4. W. Klingenstein and H. Schweizer, "Direct gap recombination in germanium at high excitation level and low temperature," Solid-State Electron. **21**, 1371–1374 (1978).
5. G. Masini, L. Colace, and G. Assanto, "2.5 Gbit/s polycrystalline germanium-on-silicon photodetector operating from 1.3 to 1.55 μm," Appl. Phys. Lett. **82**, 2524–2526 (2003).
6. G. Dehlinger, S. Koester, J. Schaub, J. Chu, Q. Ouyang, and A. Grill, "High-speed germanium-on-SOI lateral PIN photodiodes," IEEE Photon. Technol. Lett. **16**, 2547–2549 (2004).
7. Y. Kang, H.-D. Liu, M. Morse, M. J. Paniccia, M. Zadka, S. Litski, G. Sarid, A. Pauchard, Y.-H. Kuo, H.-W. Chen, W. S. Zaoui, J. E. Bowers, A. Beling, D. C. McIntosh, X. Zheng, and J. C. Campbell, "Monolithic germanium//silicon avalanche photodiodes with 340 GHz gain–bandwidth product," Nat. Photonics **3**, 59–63 (2009).
8. M. A. Green, J. Zhao, A. Wang, P. J. Reece, and M. Gal, "Efficient silicon light-emitting diodes," Nature **412**, 805–808 (2001).
9. C.-Y. Tsai, "Theoretical model for the optical gain coefficient of indirect-band-gap semiconductors," J. Appl. Phys. **99**, 053506 (2006).
10. M. V. Fischetti and S. E. Laux, "Band structure, deformation potentials, and carrier mobility in strained Si, Ge, and SiGe alloys," J. Appl. Phys. **80**, 2234–2252 (1996).
11. J. Liu, X. Sun, R. Camacho-Aguilera, L. C. Kimerling, and J. Michel, "Ge-on-Si laser operating at room temperature," Opt. Lett. **35**, 679–681 (2010).
12. R. E. Camacho-Aguilera, Y. Cai, N. Patel, J. T. Bessette, M. Romagnoli, L. C. Kimerling, and J. Michel, "An electrically pumped germanium laser," Opt. Express **20**, 11316–11320 (2012).
13. J. Liu, X. Sun, D. Pan, X. Wang, L. C. Kimerling, T. L. Koch, and J. Michel, "Tensile-strained, n-type Ge as a gain medium for monolithic laser integration on Si," Opt. Express **15**, 11272–11277 (2007).
14. S.-W. Chang and S. L. Chuang, "Theory of optical gain of Ge-Si$_x$Ge$_y$Sn$_{1-x-y}$ quantum-well lasers," IEEE J. Quantum Electron. **43**, 249–256 (2007).
15. G. Pizzi, M. Virgilio, and G. Grosso, "Tight-binding calculation of optical gain in tensile strained 001.-Ge/SiGe quantum wells," Nanotechnology **21**, 055202 (2010).

16. M. El Kurdi, G. Fishman, S. Sauvage, and P. Boucaud, "Band structure and optical gain of tensile-strained germanium based on a 30 band **k·p** formalism," J. Appl. Phys. **107**, 013710 (2010).
17. B. Dutt, D. Sukhdeo, D. Nam, B. Vulovic, Z. Yuan, and K. Saraswat, "Roadmap to an efficient germanium-on-silicon laser: strain vs. *n*-type doping," IEEE Photon. J. **4**, 2002–2009 (2012).
18. G.-E. Chang and H. H. Cheng, "Optical gain of germanium infrared lasers on different crystal orientations," J. Phys. D **46**, 065103 (2013).
19. J. Liu, L. C. Kimerling, and J. Michel, "Monolithic Ge-on-Si lasers for large-scale electronic-photonic integration," Semicond. Sci. Technol. **27**, 094006 (2012).
20. L. Carroll, P. Friedli, S. Neuenschwander, H. Sigg, S. Cecchi, F. Isa, D. Chrastina, G. Isella, Y. Fedoryshyn, and J. Faist, "Direct-gap gain and optical absorption in germanium correlated to the density of photoexcited carriers, doping, and strain," Phys. Rev. Lett. **109**, 057402 (2012).
21. X. Sun, J. Liu, L. C. Kimerling, and J. Michel, "Direct gap photoluminescence of *n*-type tensile-strained Ge-on-Si," Appl. Phys. Lett. **95**, 011911 (2009).
22. M. El Kurdi, T. Kociniewski, T.-P. Ngo, J. Boulmer, D. Debarre, P. Boucaud, J. F. Damlencourt, O. Kermarrec, and D. Bensahel, "Enhanced photoluminescence of heavily *n*-doped germanium," Appl. Phys. Lett. **94**, 191107 (2009).
23. E. Gaubas and J. Vanhellemont, "Dependence of carrier lifetime in germanium on resisitivity and carrier injection level," Appl. Phys. Lett. **89**, 142106 (2006).
24. E. Gaubas and J. Vanhellemont, "Comparative study of carrier lifetime dependence on dopant concentration in silicon and germanium," J. Electrochem. Soc. **154**, H231–H238 (2007).
25. W. G. Spitzer, F. A. Trumbore, and R. A. Logan, "Properties of heavily doped *n*-type germanium," J. Appl. Phys. **32**, 1822–1830 (1961).
26. J. I. Pankove and P. Aigrain, "Optical absorption of arsenic-doped degenerate germanium," Phys. Rev. **126**, 956–962 (1962).
27. C. Haas, "Infrared absorption in heavily doped *n*-type germanium," Phys. Rev. **125**, 1965–1971 (1962).
28. R. Newman and W. W. Tyler, "Effect of impurities on free-hole infrared absorption in *p*-type germanium," Phys. Rev. **105**, 885–886 (1957).
29. G. Grzybowski, R. Roucka, J. Mathews, L. Jiang, R. T. Beeler, J. Kouvetakis, and J. Menendez, "Direct versus indirect optical recombination in Ge films grown on Si substrates," Phys. Rev. B **84**, 205307 (2011).
30. X. Wang, H. Li, R. Camacho-Aguilera, Y. Cai, L. C. Kimerling, J. Michel, and J. Liu, "Infrared absorption of *n*-type tensile-strained Ge-on-Si," Opt. Lett. **38**, 652–654 (2013).
31. R. Jakomin, M. de Kersauson, M. El Kurdi, L. Largeau, O. Mauguin, G. Beaudoin, S. Sauvage, R. Ossikovski, G. Ndong, M. Chaigneau, I. Sagnes, and P. Boucaud, "High quality tensile-strained *n*-doped germanium thin films grown on InGaAs buffer layers by metal-organic chemical vapor deposition," Appl. Phys. Lett. **98**, 091901 (2011).
32. C.-Y. Tsai, C.-Y. Tsai, C.-H. Chen, T.-L. Sung, T.-Y. Wu, and F.-P. Shih, "Theoretical model for intravalley and intervalley free-carrier absorption in semiconductor lasers: beyond the classical Drude model," IEEE J. Quantum Electron. **34**, 552–559 (1998).
33. Y. Ishikawa, K. Wada, D. D. Cannon, J. Liu, H.-C. Luan, and L. C. Kimerling, "Strain-induced bandgap shrinkage in Ge grown on Si substrate," Appl. Phys. Lett. **82**, 2044–2046 (2003).
34. J. Menendez and J. Kouvetakis, "Type-I $Ge/Ge_{1-x-y}Si_xSn_y$ strained-layer heterostructures with a direct Ge bandgap," Appl. Phys. Lett. **85**, 1175–1177 (2004).
35. Y.-Y. Fang, J. Tolle, R. Roucka, A. V. G. Chizmeshya, J. Kouvetakis, V. R. D. Costa, and J. Menendez, "Perfectly tetragonal, tensile-strained Ge on $Ge_{1-y}Sn_y$ buffered Si (100)," Appl. Phys. Lett. **90**, 061915 (2007).
36. H. Lin, R. Chen, W. Lu, Y. Huo, T. I. Kamins, and J. S. Harris, "Structural and optical characterization of Si*x*Ge_{1-x-y}Sn*y* alloys grown by molecular beam epitaxy," Appl. Phys. Lett. **100**, 141908 (2012).
37. S. Gupta, B. Magyari-Kope, Y. Nishi, and K. C. Saraswat, "Achieving direct band gap in germanium through integration of Sn alloying and external strain," J. Appl. Phys. **113**, 073707 (2013).
38. B. Dutt, H. Lin, D. S. Sukhdeo, B. M. Vulovic, S. Gupta, D. Nam, K. C. Saraswat, and J. S. Harris, Jr., "Theoretical analysis of GeSn alloys as a gain medium for a Si-compatible laser," IEEE J. Sel. Top. Quantum Electron. **19**, 1502706 (2013).
39. Y. Bai, K. E. Lee, C. Cheng, M. L. Lee, and E. A. Fitzgerald, "Growth of highly tensile-strained Ge on relaxed $In_xGa_{1-x}As$ by metal-organic chemical vapor deposition," J. Appl. Phys. **104**, 084518 (2008).
40. Y. Hoshina, A. Yamada, and M. Konagai, "Growth and characterization of highly tensile-strained Ge on $In_xGa_{1-x}As$ virtual substrate by solid source molecular beam epitaxy," Jpn. J. Appl. Phys. **48**, 111102 (2009).
41. Y. Huo, H. Lin, R. Chen, M. Makarova, Y. Rong, M. Li, T. I. Kamins, J. Vuckovic, and J. S. Harris, "Strong enhancement of direct transition photoluminescence with highly tensile-strained Ge grown by molecular beam epitaxy," Appl. Phys. Lett. **98**, 011111 (2011).
42. J. R. Sanchez-Perez, C. Boztug, F. Chen, F. F. Sudradjat, D. M. Paskiewicz, R. Jacobson, M. G. Lagally, and R. Paiella, "Direct-bandgap light-emitting germanium in tensilely strained nanomembranes," Proc. Natl. Acad. Sci. U.S.A. **108**, 18893–18898 (2011).
43. M. de Kersauson, M. Prost, A. Ghrib, M. El Kurdi, S. Sauvage, L. Largeau, G. Beaudoin, O. Mauguin, R. Jakomin, I. Sagnes, G. Ndong, M. Chaigneau, R. Ossikovski, and P. Boucaud, "Effect of increasing thickness on tensile-strained germanium grown on InGaAs buffer layers," J. Appl. Phys. **113**, 183508 (2013).
44. P. H. Lim, S. Park, Y. Ishikawa, and K. Wada, "Enhanced direct bandgap emission in germanium by micromechanical strain engineering," Opt. Express **17**, 16358–16365 (2009).
45. A. Ghrib, M. El Kurdi, M. de Kersauson, M. Prost, S. Sauvage, X. Checoury, G. Beaudoin, I. Sagnes, and P. Boucaud, "Tensile-strained germanium microdisks," Appl. Phys. Lett. **102**, 221112 (2013).
46. M. El Kurdi, H. Bertin, E. Martincic, M. de Kersauson, G. Fishman, S. Sauvage, A. Bosseboeuf, and P. Boucaud, "Control of direct band gap emission of bulk germanium by mechanical tensile strain," Appl. Phys. Lett. **96**, 041909 (2010).
47. D. Nam, D. Sukhdeo, S.-L. Cheng, A. Roy, K. C.-Y. Huang, M. Brongersma, Y. Nishi, and K. Saraswat, "Electroluminescence from strained germanium membranes and implications for an efficient Si-compatible laser," Appl. Phys. Lett. **100**, 131112 (2012).
48. C. Boztug, J. R. Sachez-Peez, F. F. Sudradjat, R. Jacobson, D. M. Paskiewicz, M. G. Lagally, and R. Paiella, "Tensilely strained germanium nanomembranes as infrared optical gain media," Small **9**, 622–630 (2013).
49. D. Nam, D. Sukhdeo, A. Roy, K. Balram, S.-L. Cheng, K. C.-Y. Huang, Z. Yuan, M. Brongersma, Y. Nishi, D. Miller, and K. Saraswat, "Strained germanium thin film membrane on silicon substrate for optoelectronics," Opt. Express **19**, 25866–25872 (2011).
50. M. de Kersauson, M. El Kurdi, S. David, X. Checoury, G. Fishman, S. Sauvage, R. Jakomin, G. Beaudoin, I. Sagnes, and P. Boucaud, "Optical gain in single tensile-strained germanium photonic wire," Opt. Express **19**, 17925–17934 (2011).
51. A. Ghrib, M. de Kersauson, M. El Kurdi, R. Jakomin, G. Beaudoin, S. Sauvage, G. Fishman, G. Ndong, M. Chaigneau, R. Ossikovski, I. Sagnes, and P. Boucaud, "Control of tensile strain in germanium waveguides through silicon nitride layers," Appl. Phys. Lett. **100**, 201104 (2012).
52. G. Capellini, G. Kozlowski, Y. Yamamoto, M. Lisker, C. Wenger, G. Niu, P. Zaumseil, B. Tillack, A. Ghrib, M. de Kersauson, M. El Kurdi, P. Boucaud, and T. Schroeder, "Strain analysis in SiN/Ge microstructures obtained via Si-complementary metal oxide semiconductor compatible approach," J. Appl. Phys. **113**, 013513 (2013).
53. G. Shambat, S.-L. Cheng, J. Lu, Y. Nishi, and J. Vuckovic, "Direct band Ge photoluminescence near 1.6 μm coupled to Ge-on-Si microdisk resonators," Appl. Phys. Lett. **97**, 241102 (2010).
54. J. S. Xia, Y. Ikegami, K. Nemoto, and Y. Shiraki, "Observation of whispering-gallery modes in Si microdisks at room temperature," Appl. Phys. Lett. **90**, 141102 (2007).

55. R. Ossikovski, G. Picardi, G. Ndong, and M. Chaigneau, "Raman spectroscopy and polarization: selected case studies," C. R. Phys. **13**, 837–852 (2012).
56. M. El Kurdi, M. de Kersauson, A. Ghrib, M. Prost, S. Sauvage, R. Jakomin, G. Beaudoin, O. Mauguin, L. Largeau, I. Sagnes, G. Ndong, M. Chaigneau, R. Ossikovski, and P. Boucaud, "(Invited) Strain engineering for optical gain in germanium," ECS Trans. **50**, 363–370 (2013).
57. P. Boucaud, M. El Kurdi, S. Sauvage, M. de Kersauson, A. Ghrib, and X. Checoury, "Light emission from strained germanium," Nat. Photonics **7**, 162–162 (2013).
58. X. Sun, J. Liu, L. C. Kimerling, and J. Michel, "Room-temperature direct bandgap electroluminesence from Ge-on-Si light-emitting diodes," Opt. Lett. **34**, 1198–1200 (2009).
59. S.-L. Cheng, J. Lu, G. Shambat, H.-Y. Yu, K. Saraswat, J. Vuckovic, and Y. Nishi, "Room temperature 1.6 μm electroluminescence from Ge light emitting diode on Si substrate," Opt. Express **17**, 10019–10024 (2009).
60. M. de Kersauson, R. Jakomin, M. El Kurdi, G. Beaudoin, N. Zerounian, F. Aniel, S. Sauvage, I. Sagnes, and P. Boucaud, "Direct and indirect band gap room temperature electroluminescence of Ge diodes," J. Appl. Phys. **108**, 023105 (2010).
61. T.-H. Cheng, C.-Y. Ko, C.-Y. Chen, K.-L. Peng, G.-L. Luo, C. W. Liu, and H.-H. Tseng, "Competitiveness between direct and indirect radiative transitions of Ge," Appl. Phys. Lett. **96**, 091105 (2010).
62. S.-L. Cheng, G. Shambat, J. Lu, H.-Y. Yu, K. Saraswat, T. I. Kamins, J. Vuckovic, and Y. Nishi, "Cavity-enhanced direct band electroluminescence near 1550 nm from germanium microdisk resonator diode on silicon," Appl. Phys. Lett. **98**, 211101 (2011).
63. M. Oehme, M. Gollhofer, D. Widmann, M. Schmid, M. Kaschel, E. Kasper, and J. Schulze, "Direct bandgap narrowing in Ge LEDs on Si substrates," Opt. Express **21**, 2206–2211 (2013).
64. P. Velha, K. F. Gallacher, D. C. Dumas, D. J. Paul, M. Myronov, and D. R. Leadley, "Direct band-gap electroluminescence from strained n-Ge light emitting diodes," ECS Trans. **50**, 305–308 (2013).